Available online at www.sciencedirect.com
ScienceDirect
Journal of the European Ceramic Society 27 (2007) 2613–2621
www.elsevier.com/locate/jeurceramsoc

Constrained sintering of YSZ/Al_2O_3 composite coatings on metal substrates produced from eletrophoretic deposition

X.-J. Lu, P. Xiao *

School of Materials, University of Manchester, Manchester M1 7HS, UK

Received 21 April 2006; received in revised form 13 September 2006; accepted 24 September 2006
Available online 27 November 2006

Abstract

Yttria stabilized zirconia/alumina (YSZ/Al_2O_3) composite coatings were prepared from electrophoretic deposition (EPD), followed by sintering. The constrained sintering of the coatings on metal substrates was characterized with microstructure examination using electron microscopy, mechanical properties examination using nanoindentation, and residual stress measurement using Cr^{3+} fluorescence spectroscopy. The microstructure close to the coating/substrate interface is more porous than that near the surface of the EPD coatings due to the deposition process and the constrained sintering of the coatings. The sintering of the YSZ/Al_2O_3 composite coating took up to 200 h at 1250 °C to achieve the highest density due to the constraint of the substrate. When the coating was sintered at 1000 °C after sintering at 1250 °C for less than 100 h, the compressive stress was generated due to thermal mismatch between the coating and metal substrate, leading to further densification at 1000 °C because of the 'hot pressing' effect. The relative densities estimated based on the residual stress measurements are close to the densities measured by the Archimedes method, which excludes an open porosity effect. The densities estimated from the hardness and the modulus measurements are lower than those from the residual stress measurement and the Archimedes method, because it takes account of the open porosity.

Keywords: Sintering; Porosity; YSZ; Al_2O_3; Hot pressing

1. Introduction

Thermal barrier coatings (TBCs) are being used in turbines for propulsion and power generation not only to reduce heat transfer through the coating but also to protect metal components from oxidation and hot corrosion.[1–5] The currently used TBCs are yttria stabilized zirconia (YSZ) coatings which are either air plasma sprayed (APS) or deposited by electron beam physical vapor deposition (EBPVD). Compared with APS and EBPVD, electrophoretic deposition (EPD)[6] has been developed to fabricate ceramic coatings due to its advantages over the current coating techniques: the capability of producing thin and thick coatings on complex shaped substrates, the controlled microstructure, the simplicity of the process, the low equipment cost and the high deposition rate. The process involves two steps. First, the charged particles suspended in a liquid migrate towards the metal substrate (electrode) under an external dc field and deposit on the substrate to form a ceramic coating. Then, the green ceramic coating is sintered at high temperature to consolidate the coating and improve the coating/substrate adhesion. However, low sintering temperature is required to avoid damage to the metal substrate, and the sintering is constrained by the metal substrate. Hence, highly porous coatings are normally produced by using this process.[7]

The high porosity[8,9] in the TBC coatings results in higher strain tolerance and lower thermal conductivity which improves the engine performance and reliability, and gives better thermal protection, although the high porosity leads to poor mechanical strength of the coating. Thermal exposure of EBPVD and APS TBCs[10–12] to high temperature resulted in crack healing, grain growth, redistribution of pores and decreased porosity, i.e., the sintering of the ceramic coatings.[9] This sintering is detrimental to the strain tolerance, and results in an increase in thermal conductivity, which implies a loss of thermal insulation to the substrate. Therefore, the sintering of ceramic coatings is critical to their performance and reliability as TBCs. Therefore, a study of the long-term sintering behaviour of EPD coatings is essential to develop the coatings for thermal barrier applications.

* Corresponding author. Tel.: +44 161 200 5941; fax: +44 161 200 3586.
E-mail address: Ping.xiao@manchester.ac.uk (P. Xiao).

0955-2219/$ – see front matter © 2006 Elsevier Ltd. All rights reserved.
doi:10.1016/j.jeurceramsoc.2006.09.016

Sintering of ceramic coatings on substrates is different from free materials due to the presence of the substrate. The constraint of the substrate[13–17] leads to a lower densification rate in constrained coatings, therefore, a lower density and larger pores in constrained coatings. The lower densification rate has been reported in a gold circuit paste on alumina substrate,[15] borosilicate glass on silicon substrate,[14] alumina/glass/alumina sandwich structure[18] and alumina/borosilicate glass + alumina/alumina sandwich structure.[19] Constrained sintering also led to crack growth and damage in glass and Al_2O_3 films on various substrates,[16] flaw generation in multilayer films,[20] larger pores in a constrained glass film[14] and along the interface between the glass-ceramic and silicon substrate,[21] higher porosity in constrained films.[15,19]

In this work, the YSZ/Al_2O_3 ceramic coatings have been fabricated on Fecralloy substrates using EPD then sintered at 1250 °C for 4 h. Long-term sintering was carried out both at 1250 and 1000 °C. Microstructural evolution, residual stress development and changes in mechanical properties have been examined in relation to the sintering condition. The overall density measured by the Archimedes and weight–volume methods was compared with those estimated from residual stress, hardness and modulus measurements. The sintering mechanism under a compressive stress and the constrained sintering mechanism are discussed.

2. Experimental

2.1. Sample preparation

A mixture of 95 wt.% YSZ powder (~0.3 μm, HSY-8, Daiichi Kigenso Kagaku Kogyo, Japan) and 5 wt.% Al powder (<6 μm, Alpoco, UK) was attrition-milled in acetylacetone (Aldrich, UK) for 8 h. The attrition mill (type 01HD, Szegvari Attrior system, Union Process), which has a 750-cc capacity milling tank, was charged with 40 g of powder, 800 g of tetragonal zirconia polycrystal (TZP) milling balls with diameter of 3 mm and 200 ml of acetylacetone. The stirring arm was maintained at a rotational speed of 450 rpm. After milling, the suspension was diluted in acetylacetone to a solid loading of 6 wt.%. EPD was carried out by applying an electric field between a platinum electrode (as anode) and a Fecralloy substrate (cathode). The Fecralloy plate has dimension of 25 mm × 10 mm × 1 mm (Fe–22% Cr–5% Al–1% Y–1% Zr, Goodfellow, UK). During EPD, the suspension was kept stirred using a magnetic stirrer and a constant voltage of 80 V was applied between the two electrodes. The green coatings were dried at room temperature for 24 h before they were sintered in air at 1250 °C for 4 h, which are termed as-sintered coatings. During heating to 1250 °C, the Al in YSZ was oxidized into Al_2O_3, and the YSZ/Al_2O_3 composite coating was then sintered at 1250 °C. Meanwhile, oxygen can penetrate through the composite coating to oxidize the Fecralloy substrate, producing an alumina layer, also called thermally grown oxide (TGO), between the coating and substrate. To study the long-term sintering effect, the as-sintered coatings were further treated in a carbolite furnace CF-1300 at 1000 °C for 33, 100, 200, 300 and 500 h and at 1250 °C for 30, 100, 200, 300 and 400 h, respectively. The heating and cooling rates were both 3 °C/min.

2.2. Characterization

A nano-indenter® XP (Nano Instruments, MTS Systems Corporation, USA) was used to measure the mechanical properties of the samples. Indentation was made using a Berkovich indenter. The tip geometry of the indenter was calibrated with a standard silica specimen by running a standard continuous stiffness measurement (CSM).[22] The load was held at 70% of a maximum load for a given penetration depth for 100 s to correct the thermal drift. Hardness and Young's modulus were determined from the unloading profile using the Oliver and Pharr analysis method.[22] All the measurements on the top surface were made up to 2 μm penetration depth. With penetration depth of 1–2 μm consistent results were generated. To avoid interference between two adjacent measurements and maximize number of positions being measured, 1 μm penetration depth was chosen for the cross-section measurements.

The residual stress was measured using the Cr^{3+} fluorescence spectroscopy. The instrumentation consisted of a modified optical microscope (Nikon), a laser system (He–Ne, 632.8 nm wave length, 15 mW power), a double spectrometer (Glen, Creston) and a charge-coupled device camera (CCD, Wright Instruments, Peltier cooled). An X50 objective lens and 2 s collecting time were used for all the measurements. The laser was focused at a position along the cross-section of the coatings and the laser spot size was set about 2–5 μm. By illuminating laser at the top surface of a wedged coating on a substrate, fluorescence signal was generated either only from the coating itself when the laser probing depth is less than the coating thickness, or from both the coating and the alumina layer underneath when the coating thickness is less than the probing depth. By measuring the fluorescence spectra across the wedged surface of the coating, the probe depth into the coating was determined as 10 μm by measuring the thickness of coating when the fluorescence signal starts to come from both the TGO and the coating. The R-line spectra were recorded and analyzed by commercial software (Renishaw Wire). The spectra were fitted by Gaussian–Lorentzian functions.

After removal of the metal substrate in hydrochloric acid, the residual stresses in the free-standing coating caused by the mismatch between the Al_2O_3 particles and the matrix YSZ coating exist locally around individual Al_2O_3 particles, which are termed as micro-stresses. The micro-stresses were assumed to be hydrostatic, the dependence of the wavenumber shift ($\Delta\nu_{micro}$) of the R peaks in the fluorescence spectra upon micro-stress is given by[23]

$$\Delta\nu_{micro} = 7.61\sigma_{micro} \quad (1)$$

The densities of samples were measured by the Archimedes method and also achieved by measuring weight and dimensions of the samples (termed as weight–volume method). The microstructures of samples were examined by scanning electron microscopy (XL30, Philips).

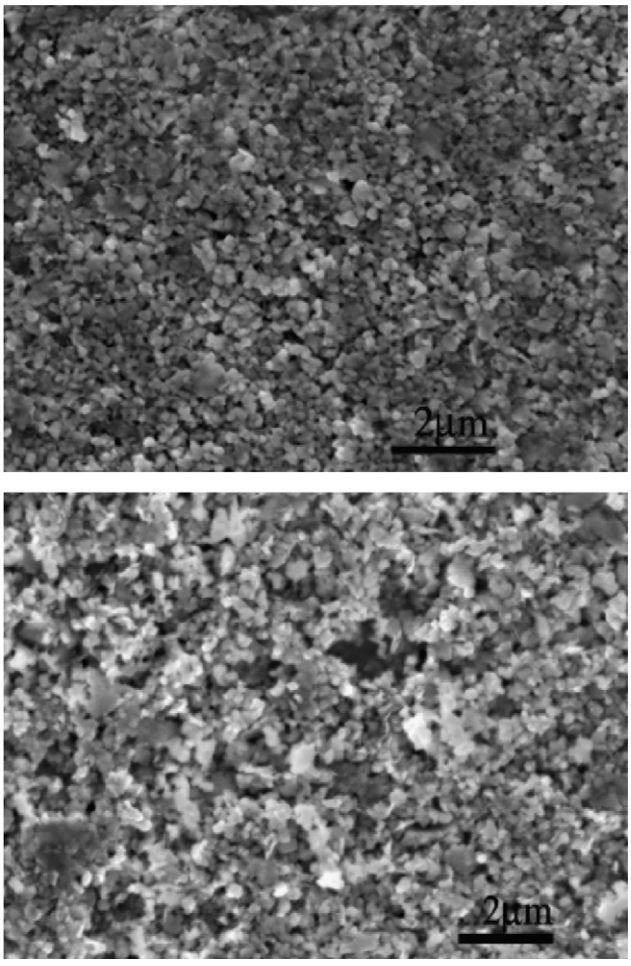

Fig. 1. SEM images of a green YSZ/Al EPD coating: (a) top surface; (b) underside face.

3. Results

3.1. Microstructures of YSZ/Al_2O_3 composite coatings

Fig. 1 shows SEM images of the top surface and the underside face of the green coating produced from EPD and drying. The underside of the green coating is in a looser packing and the particles are larger than that of the top surface. Fig. 2 shows a fractured cross-section of a coating after sintering at 1250 °C for 4 h. The reason to examine fractured surface instead of polished one is that polishing of the porous coating would lead to filling of pores and underestimation of the porosity. According to the image of the cross-section, particularly the high magnification images, the area near the interface is rougher than that near the top surface which indicates that the region close to the interface is more porous. The region within 30 μm of the interface of the coatings appears to be rougher than the rest of the coating. The density of the as-sintered coating was measured as 72% by the Archimedes method, which excludes the open pores. The density of the as-sintered coating was measured as 59% by the weight–volume method, which includes both close pores and open pores.

The as-sintered YSZ/Al_2O_3 EPD coatings were further treated at 1000 °C for various times. Fig. 3 shows the top surfaces of the as-sintered coatings and the thermally treated coatings at 1000 °C for 500 h. After 500 h thermal treatment at 1000 °C, density of the coating, measured using the Archimedes method, increased from 72% to 76% while the density measured by the weight–volume method increased from 59% to 61%.

3.2. Mechanical properties

3.2.1. Sintering at 1000 °C

The mechanical properties of the coating were measured using nanoindentation. The hardness along the cross-section of the as-sintered coating increased dramatically from the coating/substrate interface up to a distance of 30 μm and increased slightly up to the top surface of the coating (Fig. 4). A similar trend was observed for the coatings after thermal treatment at 1000 °C for 33 h, although the hardness of the thermally treated coating is higher than that of the as-sintered one. This variation of the hardness along the coating thickness is attributed to the change in microstructure of the coating along its thickness (Fig. 2) where the porous structure is present at the region within the distance of 30 μm from the interface. The Young's modulus of the coating shows a similar trend as that of the hardness of the coating (Fig. 5).

The change in both the hardness and the Young's modulus of the coating after the thermal treatments at 1000 °C indicates that sintering occurred at 1000 °C. Fig. 6 shows the hardness and Young's modulus of the coating as a function of the thermal treatment time at 1000 °C where measurements were made at locations with different distances from the interface. In all of the locations, both the hardness and Young's modulus increased with an initial treatment for 33 h. It should be noted the sintering occurred at 1000 °C within 33 h, but further treatments after 33 h led to little extra sintering.

To study the constraint effect of the substrate on sintering, the green coatings on substrates were first sintered at 1250 °C for 4 h (termed as C1). Then the coatings C1 were thermally treated at 1000 °C for 30 h (C2). In comparison, the substrate of the coating C1 was removed and then sintered at 1000 °C for 30 h as a free-standing coating (R1). Alternatively, a green free-standing YSZ/Al coating, which was produced after removal of the substrate after EPD, was first sintered at 1250 °C for 4 h (F1). Then the F1 was further thermally treated at 1000 °C for 30 h (F2). The hardness and the Young's modulus of these coatings are shown in Fig. 7. Compared with C1, the hardness of C2 increased slightly from 3.58 to 3.79 GPa after the further thermal treatment, which meant C1 was further densified at 1000 °C after 30 h. The R1 achieved a higher hardness and Young's modulus not only than that of C1 and C2, but also is close to that of F1. The F1 has completed densification at 1250 °C within 4 h and cannot be further densified with further thermal treatment at 1000 °C for 30 h (F2). The hardness and Young's modulus of the F2 is similar to that of F1. Therefore, the substrate constraint hindered sintering at 1250 °C. Without a substrate, sintering at 1250 °C was completed within 4 h.

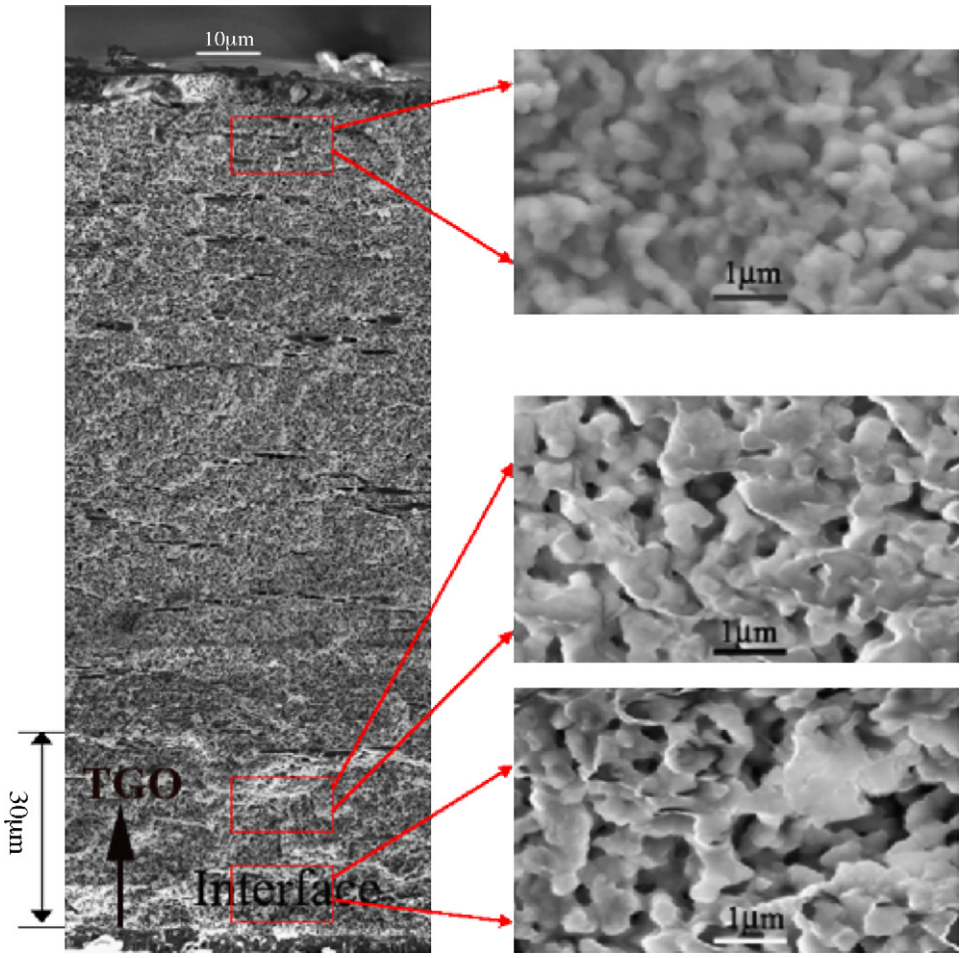

Fig. 2. Cross-section of the fractured as-sintered YSZ/Al_2O_3 EPD coating.

3.2.2. Long-term sintering at 1250 °C

The as-sintered coatings were further sintered at 1250 °C for various times, and then each sample was thermally treated at 1000° for 30 h. The hardnesses and Young's moduli are shown in Fig. 8. The hardnesses and the Young's moduli of the coatings increased with sintering times up to 200 h at 1250 °C. After 200 h at 1250 °C, both hardness and Young's modulus become constant. 30-h treatment at 1000 °C led to an increase in the hardness and the Young's modulus of the coating sintered at 1250 °C for 100 h to the level achieved by sintering at 1250 °C for 200 h.

The free-standing YSZ/Al_2O_3 coating completed sintering within 4 h at 1250 °C as shown in Section 3.2.1. The long-term sintering at 1250 °C indicates the supported YSZ/Al_2O_3 EPD coating takes a longer time to reach the sintering equilibrium due to the constraint of the substrate.

3.3. Residual stress

As described in previous papers,[23,24] the micro-stress was generated due to thermal mismatch between the Al_2O_3 and YSZ in the coating, and indicates the density of the coating, therefore degree of sintering. The micro-stresses in the Al_2O_3 phase are compressive as the thermal expansion coefficient of YSZ is higher than that of the Al_2O_3. Fig. 9(a) shows the micro-stresses of the as-sintered coatings and the thermally treated coatings as a function of the distance from the interface. The micro-stresses in the thermally treated coating are larger than those of the as-sintered coating, confirming further sintering occurred at 1000 °C. In addition, the increase of the micro-stresses is larger at positions close to the top surface than those close to the interface, confirming that the constraint effect of sintering is larger at the interface than that at the surface of the coating. The micro-stresses in the coating at different locations increased with an initial thermal treatment of 33 h, then became stable with further treatments, which is consistent with results from the measurements of mechanical properties. It should be noted that the presence of the alumina layer (TGO) attached to the coating after the removal of the substrate may affect the stress in the coating. But its effect has not been considered here.

4. Discussion

4.1. Sintering under compressive stresses

The incomplete sintering at 1250 °C for 4 h provides a possibility for further densification of the supported YSZ/Al_2O_3 EPD coating. Even after 100 h thermal treatment at 1250 °C, the

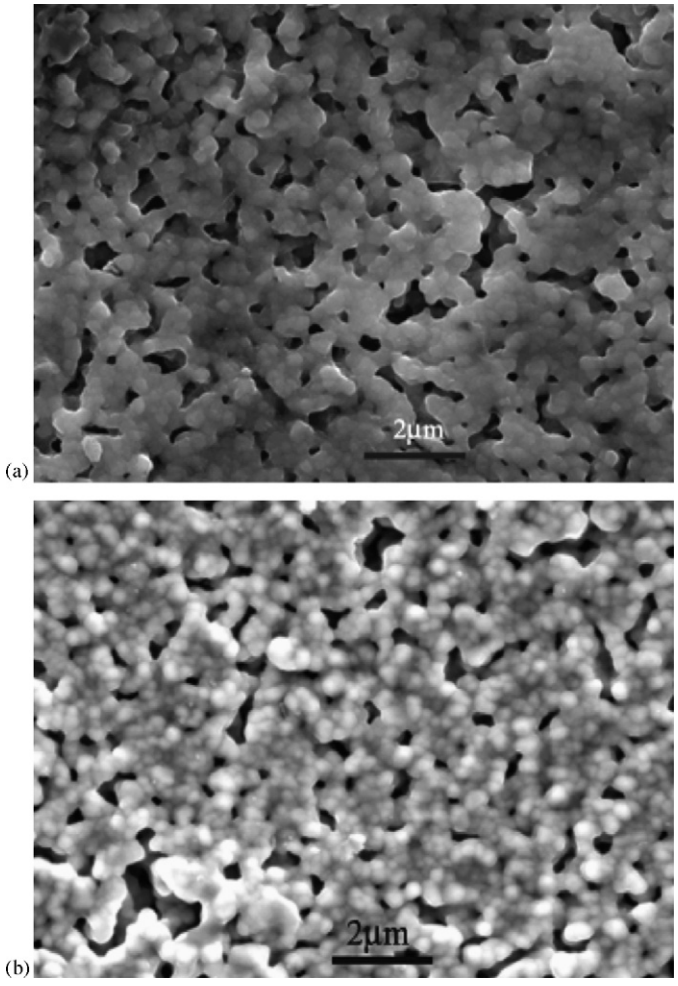

Fig. 3. SEM images of the as-sintered and the thermally treated YSZ/Al_2O_3 EPD coatings: (a) as-sintered; (b) top surface of the thermally treated coating at 1000 °C for 500 h.

YSZ/Al_2O_3 EPD coating was still further densified after 30 h at 1000 °C (Fig. 8). A shorter time treatment at a lower temperature (1000 °C for 30 h) after a longer time at a higher temperature (1250 °C for 100 h) achieved almost the same hardness and Young's modulus as achieved by 200 h sintering at 1250 °C.

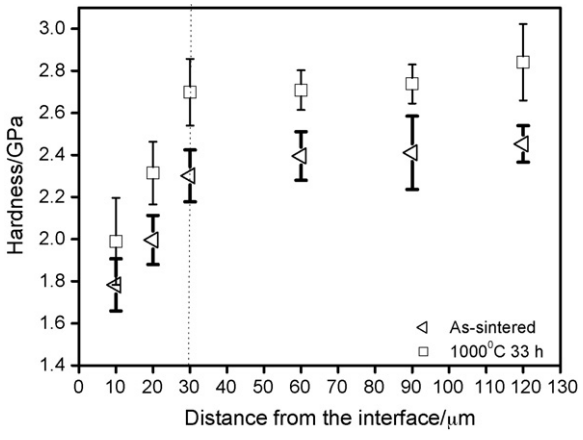

Fig. 4. The hardness of the as-sintered and the thermally treated supported YSZ/Al_2O_3 EPD coating at 1000 °C for 33 h.

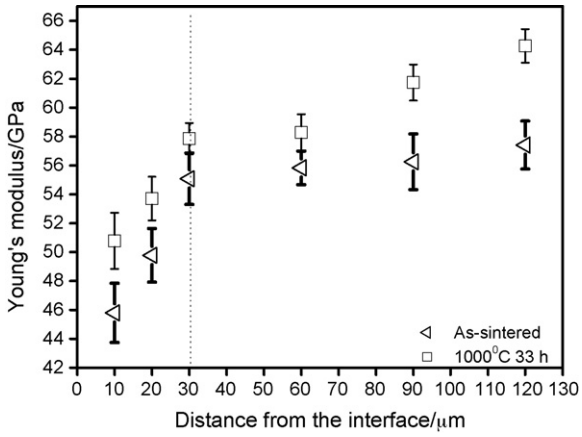

Fig. 5. The Young's modulus of the as-sintered and the thermally treated supported YSZ/Al_2O_3 EPD coating at 1000 °C for 33 h.

The further densification at 1000 °C may be contributed by the compressive stresses in the supported coatings.

In this study, the supported YSZ/Al_2O_3 composite coatings were thermally treated at 1000 °C, which is lower than the frozen temperature (1200 °C),[25] below which the stresses cannot be relaxed anymore and then started to build up. Then a compressive stress was induced upon cooling down from the high sintering

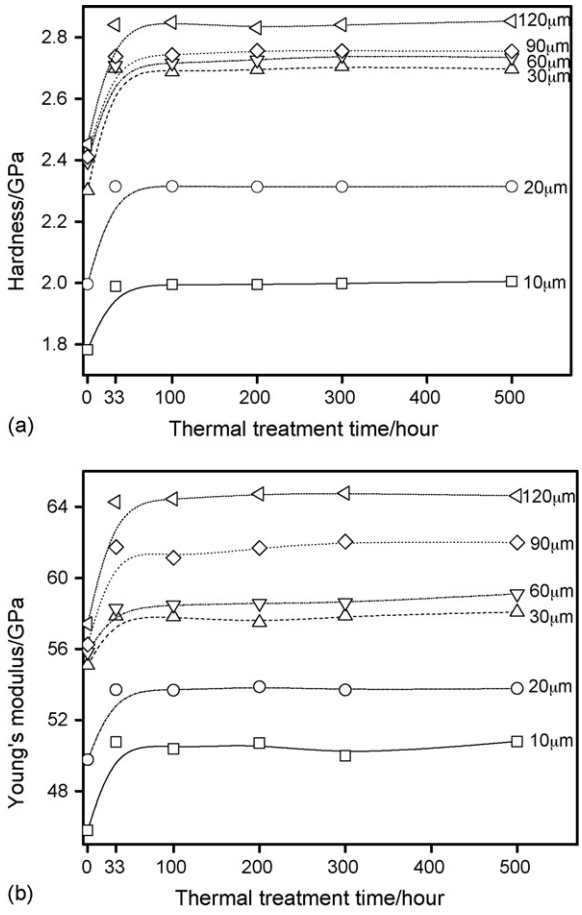

Fig. 6. Hardness (a) and Young's modulus (b) as a function of thermally treated times at different distances from the interface (thermally treated temperature is 1000 °C).

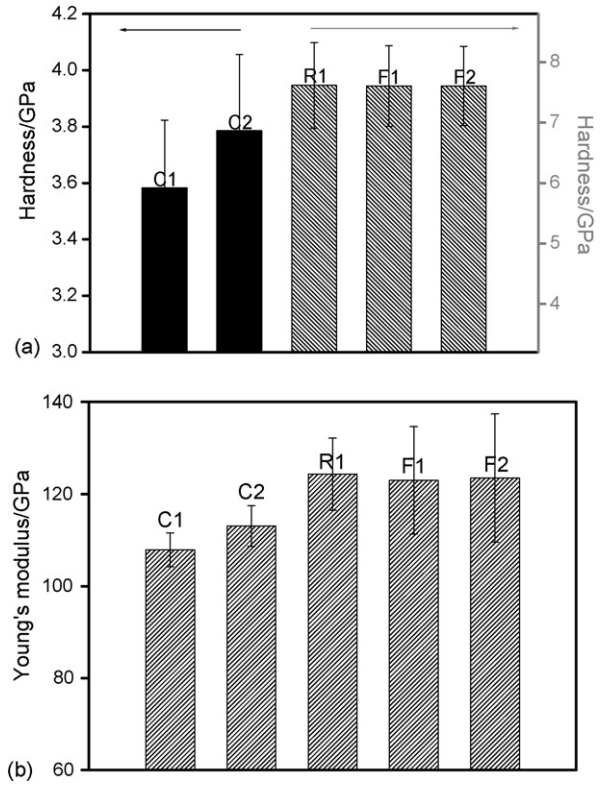

Fig. 7. Hardness (a) and Young's modulus (b) of the YSZ/Al_2O_3 EPD coating (C1, green supported coating sintered at 1250 °C for 4 h; C2, C1 after 30 h thermal treatment at 1000 °C; R1, green supported coating sintered at 1250 °C for 4 h and then removed substrate to be thermally treated at 1000 °C for 30 h; F1, green free-standing coating sintered at 1250 °C for 4 h; F2, F1 after 30 h thermal treatment at 1000 °C.

temperature of 1250 to 1000 °C. Assuming both the coating and Fecralloy are elastic from 1200 to 1000 °C, the compressive stress can be calculated by[26]

$$\sigma = \frac{E_c(\alpha_c - \alpha_s)\Delta T}{1 - \nu_c} \quad (2)$$

where E_c and ν_c are the elastic modulus and Poisson ratio of the coating, α the coefficient of thermal expansion, the subscripts, 'c' and 's', refer to the coating and substrate, respectively, and ΔT is the temperature change. The retained compressive stress cooling down from the frozen temperature 1200 to 1000 °C is calculated as 80 MPa, for which, E_c was measured as 107 GPa, ν_c is 0.23.[27] The average CTE for Fecralloy and a YSZ/Al_2O_3 composite in the range 25–1200 °C is 14.0×10^{-6} and 11.1×10^{-6} according to the literature.[26,28] It should be noted that creep of both the coating and Fecralloy was ignored here, so the stress value is overestimated. However, the compressive stresses could be up to 80 MPa.

The driving force[29–32] for sintering is related to the curvature of the particles/grains which in turn is related to surface energy:

$$\sigma_s = \frac{2\gamma}{r} + \frac{2\gamma_b}{G} \quad (3)$$

where γ_b is the grain boundary energy, G the grain size, γ the surface energy and r is the pore radius of curvature. The smaller

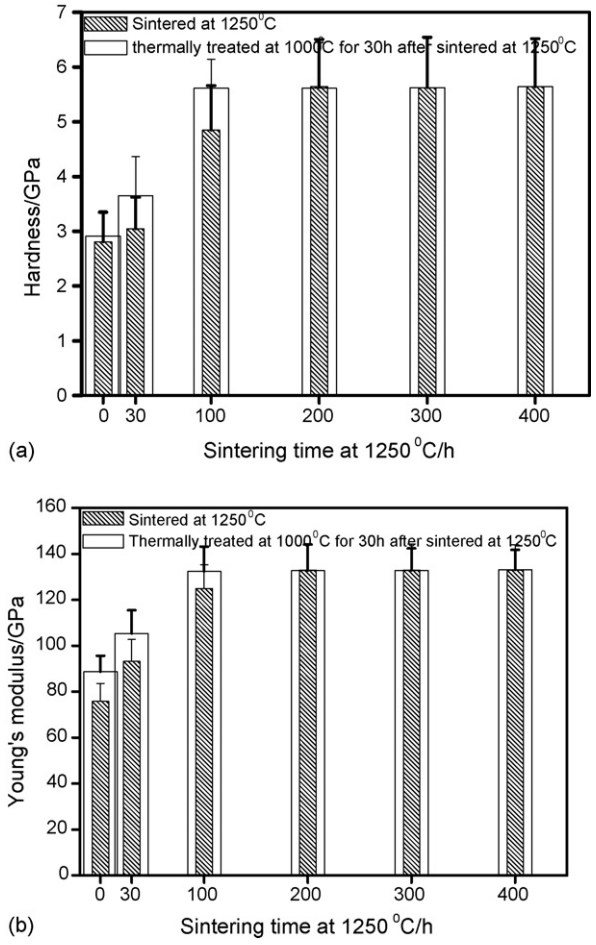

Fig. 8. The hardnesses (a) and Young's moduli (b) of sintered YSZ/Al_2O_3 EPD coatings at 1250 °C for various times and thermally treated YSZ/Al_2O_3 EPD coatings at 1000 °C for 30 h (0 h in the figure means the one as-sintered at 1250 °C for 4 h).

the particles/grains, the higher the free energy, and then the easier to be sintered. According to Tsoga and Nikolopoulos,[33] the surface energy as a function of temperature is given by

$$\gamma = 1.927 - 0.428 \times 10^{-3} T \quad (4)$$

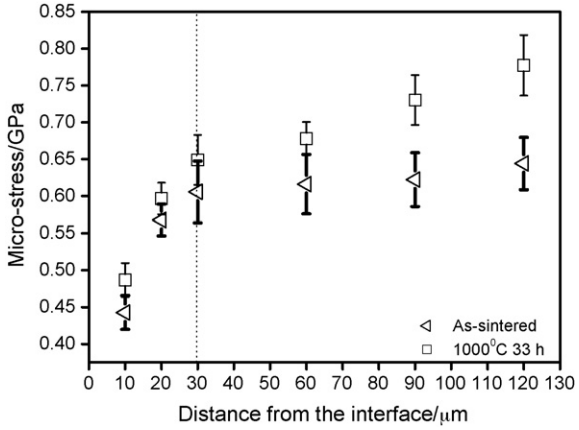

Fig. 9. Micro-stress of as-sintered and thermally treated YSZ/Al_2O_3 EPD coatings at 1000 °C as a function of distance from the interface.

and the grain-boundary energy is

$$\gamma_b = 1.215 - 0.358 \times 10^{-3} T \quad (5)$$

Then the surface energy is calculated as 1.383 J/m^2 and the grain boundary energy is 0.759 J/m^2 at 1000 °C. The surface energy and the grain boundary energy are estimated values because the equations were obtained in the temperature range 1300–1600 °C. The grain size G is measured as 0.3–0.6 μm and the curvature at the inter-particle neck is 0.05–0.6 μm. The sintering stress can be calculated as 5.875–60.38 MPa according to Eq. (3). The estimated compressive stress of 80 MPa at 1000 °C according to Eq. (2) is comparable to the sintering stress. Sintering during the application of an external pressure (P_e) is called hot pressing. A mechanical pressure can increase the driving pressure for densification (P_T) by acting against the internal pore pressure (P_i), without the increasing driving force for grain growth[34,35]:

$$P_T = P_e + \frac{2\gamma}{r} - P_i \quad (6)$$

4.2. Constraint effect

The supported YSZ/Al_2O_3 coatings densified at 1250 °C up to 200 h. The low densification rate is due to the presence of the constraint effect. Constraint sintering models[36–38] have been proposed by assuming the material followed a viscous behaviour during sintering. For the free-sintering case, the densification rate of the free sintering body can be expressed as[37,38]

$$-\frac{\dot{\rho}}{\rho} = 3\dot{\varepsilon} = \frac{\sigma_s}{K_v} \quad (7)$$

where $-\dot{\rho}/\rho$ refers to the densification rate, K_v and $\dot{\varepsilon}$ are the bulk viscosity and strain rate, respectively.

When the sintering was constrained,[13,37] the densification rate of the constrained sintering body can be expressed as

$$-\frac{\dot{\rho}}{\rho} = \frac{\sigma_s - (2/3)\sigma_{con}}{K_v} \quad (8)$$

where σ_{con} is the tensile stress generated by the constraint.

The constrained sintering leads to a reduction in the densification rate.[13,15,16,19,37] Therefore, the sintering of the supported YSZ/Al_2O_3 coatings took a long time at 1250 °C.

4.3. Density measurements

According to the model proposed by *Aahmy et al.*,[39,40] the thermal mismatch stress in a two-phase composite which contains a volume fraction (x) of inclusion phase can be expressed as

$$\sigma_{micro} = \frac{-(\alpha_i - \alpha_m)\Delta T}{(2x(1-2\nu_m) + (1+\nu_m))/(2E_m(1-x)) + (1-2\nu_i)/(E_i)} \quad (9)$$

where E_m and E_i are the Young's moduli of the matrix and the inclusion phase, ν_m and ν_i are the Poisson's ratio of the matrix and the inclusion phase, respectively, α_m and α_i are the CTE of the matrix and the inclusion phase, and x is the volume fraction of the inclusion phase.

The Young's modulus of the porous body ($P \leq 0.5$) can be related to the porosity by the Gibson and Ashby solution.[41,42] It should be noted that this equation was developed to calculate the micro-stress in a fully dense composite, therefore, the porosity in the coatings may introduce errors in use of Eq. (9). In addition of the spherical including phase was assumed in the original deduction of Eq. (9), whereas the alumina particles embedded in YSZ matrix here are irregular shape. However, the use of Eq. (9) enable us to estimate the local density in the coating according to Eq. (12), which will be compared with the density measured by using other methods:

$$E_m = E_0 e^{-bP} \quad (10)$$

where E_0 is the Young's modulus at zero porosity, P the porosity fraction, and b is an empirical constant which is associated with the fabrication technique.

Therefore the dependence of the Young's modulus on density can be expressed by

$$E_m = E_0 e^{-b(1-(\rho/\rho_0))} \quad (11)$$

where ρ is the density of porous materials and ρ_0 is the theoretical density. Based on the assumption that the mixture of the YSZ and pores is the matrix and the embedded alumina is fully dense, the density of the YSZ matrix in the coating can be obtained according to Eq. (12):

$$\sigma_{micro} = \frac{-(\alpha_i - \alpha_m)\Delta T}{(2x(1-2\nu_m) + (1+\nu_m))/(2(1-x)E_0 e^{-b(1-(\rho/\rho_0))}) + (1-2\nu_i)/(E_i)} \quad (12)$$

where E_0 and E_i are the Young's moduli of the fully dense YSZ and the inclusion phase Al_2O_3, which is taken as 205[27] and 402 GPa[28], respectively, ρ and ρ_0 are the density of the porous YSZ matrix and the theoretical density of the YSZ, respectively ($\rho_0 = 5.99$ g/cm^3),[43] ν_m and ν_i are the Poisson's ratios of the matrix YSZ and the alumina, respectively (both taken as 0.23[27,28]), α_m and α_i are the CTE of the matrix YSZ and the inclusion phase Al_2O_3, which are 11.1×10^{-6} and 8.2×10^{-6} respectively,[28,44] x the volume fraction of the Al_2O_3, which is 0.075 and b is the empirical constant. To calculate b in Eq. (10), a fully dense YSZ/Al_2O_3 composite sample was made by cold pressing of the YSZ/Al powder under pressure of 10 MPa, then the oxidation and sintering took place up to and then remained at 1400 °C for 4 h. E and E_0 were measured using nanoidentation as 107 GPa (Fig. 7(b)) and 254 GPa, respectively, for a porous YSZ/Al_2O_3 coating with a relative density of 59% and a fully dense YSZ/Al_2O_3 composite. b was then calculated as 2.10 according Eq. (10).

The relationship between hardness and porosity can be expressed as[45]

$$H = H_0(1-\theta)^2 e^{(-\beta\theta)} \quad (13)$$

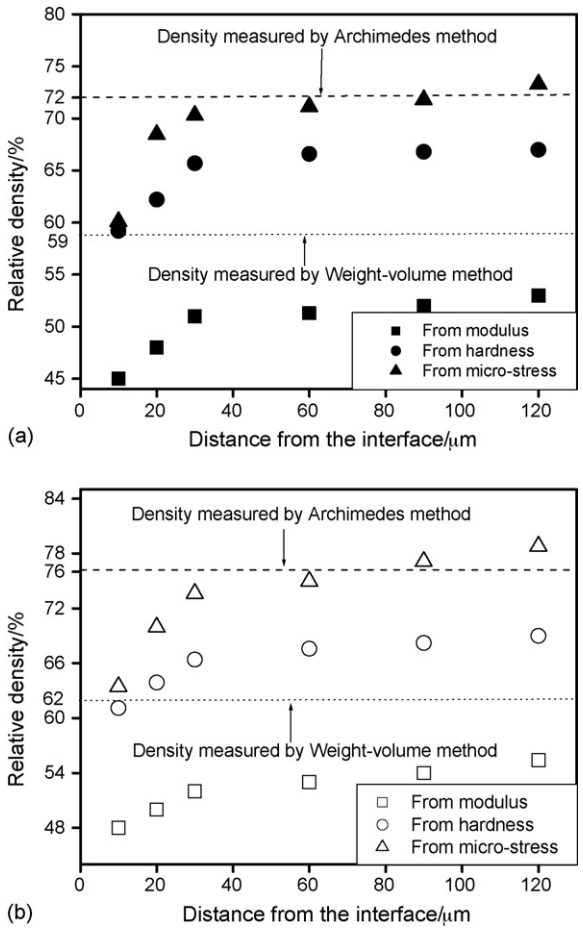

Fig. 10. The measured and calculated densities of the as-sintered and the thermally treated coating: (a) as-sintered; (b) 1000 °C 33 h.

where H_0 is the hardness at zero porosity, θ the fractional porosity, and β is the empirical constant range from 0 to 1. The hardness of a porous YSZ/Al_2O_3 coating with a relative density of 59% and a fully dense YSZ/Al_2O_3 composite were measured as 3.5 GPa (Fig. 7(a)) and 13 GPa, respectively. Then β is calculated as 0.3.

The densities across the thickness of the coating were calculated according to Eqs. (10), (12) and (13), respectively. The calculated relative densities of the as-sintered coating and coatings thermally treated at 1000 °C for 33 h are shown in Fig. 10. The densities increase from the interface to the top surface for both the as-sintered and the thermally treated ones, which is consistent with SEM observations. The relative densities calculated from the hardness and the moduli are much lower compared with the measured density by the Archimedes method. This is because the densities measured by the Archimedes method are overestimated resulting from the excluded open pores. Compared with the densities calculated from the modulus and hardness, the densities from the micro-stresses are close to the density measured by the Archimedes method. The micro-stresses, which arise from the mismatch between the YSZ and Al_2O_3 particles, present a local property excluding the open porosity effect. The density calculated from the hardness and modulus take account of the open porosity effect and approached the densities measured by the weight–volume method which includes the open porosity effect.

5. Conclusions

1. SEM, nanoindentation and residual stress measurements can be used to monitor the sintering of TBCs after thermal treatments.
2. The YSZ/Al_2O_3 coating fabricated by EPD had a graded structure across the thickness.
3. The sintering of the supported YSZ/Al_2O_3 EPD coatings take a longer time at 1250 °C due to the reduction of the densification rate by the constraint of the substrate.
4. The supported YSZ/Al_2O_3 EPD coatings sintered at 1250 °C can be further densified at 1000 °C and this further densification was attributed to the presence of the compressive thermal mismatch stress.
5. The as-sintered coating can be further sintered after removal of the substrate, and therefore, the removal of substrate constraint.
6. The relative densities calculated from the micro-stresses are close to the densities measured by the Archimedes method, which excludes open porosity effect. The densities calculated from the hardness and the modulus were lower than those calculated from the micro-stresses and Archimedes methods, but close to the densities measured by the weight–volume method which accounts for the open porosity effect.

Acknowledgments

The authors would like to thank Prof. R. Young for the use of the spectroscopy instrument in his laboratory. This research is supported by EPSRC under contract no. GR/R32215.

References

1. Miller, R. A., Current status of thermal barrier coatings—an overview. *Surf. Coat. Technol.*, 1987, **30**, 1.
2. Evans, A. G., Mumm, D. R., Hutchinson, J. W., Meier, G. H. and Pettit, F. S., Mechanisms controlling the durability of thermal barrier coatings. *Prog. Mater. Sci.*, 2001, **46**, 505.
3. Schlichting, K. W., Padture, N. P., Jordan, E. H. and Gell, M., Failure modes in plasma-sprayed thermal barrier coatings. *Mater. Sci. Eng. A*, 2003, **342**, 120.
4. Jones, R. L., *Metallurgical and Ceramic Coatings*. Chapman & Hall, London, 1996, p. 194.
5. Padture, N. P., Gell, M. and Jordan, E. H., Thermal barrier coatings for gas-turbine engine applications. *Science*, 2002, **296**, 280.
6. Wang, Z., Shemilt, J. and Xiao, P., Fabrication of ceramic composite coatings using electrophoretic deposition, reaction bonding and low temperature sintering. *J. Eur. Ceram. Soc.*, 2002, **22**, 183.
7. Ma, J., Wang, C. and Peng, K. W., Electrophoretic deposition of porous hydroxyapatite scaffold. *Biomaterials*, 2003, **24**, 3505.
8. Mcpherson, R., A Review of microstructure and properties of plasma sprayed ceramic coating. *Surf. Coat. Technol.*, 1989, **39/40**, 173.
9. Cernuschi, F., Lorenzoni, L., Ahmaniemi, S., Vuoristo, P. and Mantyla, T., Studies of the sintering kinetic of thick thermal barrier coatings by thermal diffusivity measurements. *J. Eur. Ceram. Soc.*, 2005, **25**, 393.
10. Guo, S. and Kagawa, Y., Effect of thermal exposure on hardness and Young's modulus of EB-PVD yttria-partially-stabilized zirconia thermal barrier coatings. *Ceram. Int.*, 2006, **32**, 263.

11. Thompson, J. A. and Clyne, T. W., The effect of heat treatment on the stiffness of Zirconia top coats in plasma-sprayed TBCs. *Acta Mater.*, 2001, **49**, 1565.
12. Renteria, A. F. and Saruhan, B., Effect of ageing on microstructure changes in EB-PVD manufactured standard YSZ top coat of thermal barrier coatings. *J. Eur. Ceram. Soc.*, 2006, **26**, 2249.
13. Bordia, R. K. and Raj, R., Sintering behavior of ceramic films constrained by a rigid substrate. *J. Am. Ceram. Soc.*, 1985, **68**, 287.
14. Bang, J. and Lu, G.-Q., Constained-film sintering of a borosilicate glass: *in situ* measurement of film stresses. *J. Am. Ceram. Soc.*, 1995, **78**, 813.
15. Choe, J. W., Calata, J. N. and Lu, G.-Q., Constrained-film sintering of a gold circuit paste. *J. Mater. Res.*, 1995, **10**, 986.
16. Bordia, R. K. and Jagota, A., Crack growth and damage in constrained sintering films. *J. Am. Ceram. Soc.*, 1993, **76**, 2475.
17. Garino, T. J. and Bowen, H. K., Kinetics of constrained-film sintering. *J. Am. Ceram. Soc.*, 1990, **73**, 251.
18. Tzeng, S.-Y. and Jean, J.-H., Stress development during constrained sintering of alumina/glass/alumina sandwich structure. *J. Am. Ceram. Soc.*, 2002, **85**, 335.
19. Lin, Y.-C. and Jean, J.-H., Constrained densification kinetics of alumina/borosilicate glass + alumina/alumina sandwich structure. *J. Am. Ceram. Soc.*, 2002, **85**, 150.
20. Cheng, T. and Raj, R., Flaw generation during constrained sintering of metal–ceramic and metal–glass multilayer films. *J. Am. Ceram. Soc.*, 1989, **72**, 1649.
21. Calata, J. N., Matthys, A. and Lu, G.-Q., Constrained-film sintering of Cordierite glass-ceramic on silicon substrate. *J. Mater. Res.*, 1998, **13**, 2334.
22. Oliver, W. C. and Pharr, G. M., An improved technique for determining hardness and elastic modulus using load and displacement sensing indentation experiments. *J. Mater. Res.*, 1992, **7**, 1564.
23. Wang, X. and Xiao, P., Residual stresses and constrained sintering of YSZ/Al_2O_3 composite coatings. *Acta Mater.*, 2004, **52**, 2591.
24. Lu, X.-J., Wang, X. and Xiao, P., Nanoindentation and residual stress measurements of yttria-stablized zirconia composite coatings produced by electrophoretic deposition. *Thin Solid Films*, 2005, **494**, 223.
25. Sergo, V., Wang, X. L., Clarke, D. R. and Becher, P. F., Residual stresses in alumina/ceria-stabilized zirconia composites. *J. Am. Ceram. Soc.*, 1995, **78**, 2213.
26. Tolpygo, V. K. and Clarke, D. R., Wrinkling of alumina films grown by thermal oxidation. I. Quantitative studies on single crystals of Fe–Cr–Al alloy. *Acta Mater.*, 1998, **46**, 5153.
27. Shackelford, J. F. and Alexander, W., *CRC Materials Science and Engineering Handbook*. CRC Press, New York, 2001, p. 766.
28. Green, D. J., *An Introduction to the Mechanical Properties of Ceramics*. Cambridge University Press, Cambridge, 1998, p. 25.
29. Raj, R., Analysis of the sintering pressure. *J. Am. Ceram. Soc.*, 1987, **70**, C210.
30. Shi, J. L., Relation between coarsening and densification in solid-state sintering of ceramics. *J. Mater. Res.*, 1999, **14**, 1389.
31. Shi, J. L., Thermodynamics and densification kinetics in solid-state sintering of ceramics. *J. Mater. Res.*, 1999, **14**, 1398.
32. Chen, I.-W. and Wang, X.-H., Sintering dense nanocrystalline ceramics without final-stage grain growth. *Nature*, 2000, **404**, 168.
33. Tsoga, A. and Nikolopoulos, P., Surface and grain-boundary energies in yttria-stabilized zirconia. *J. Mater. Sci.*, 1996, **31**, 5409.
34. Reed, J. S., *Principles of Ceramics Processing* (*2nd ed.*). John Wiley& Sons Inc., New York, 1995, p. 617.
35. Zuo, R., Aulbach, E., Bordia, R. K. and Rodel, J., Critical evaluation of hot forging experiments: case study in alumina. *J. Am. Ceram. Soc.*, 2003, **86**, 1099.
36. Svoboda, J., Riedel, H. and Zipse, H., Equilibrium pore surfaces, sintering stresses and constitutive equations for the intermediate and late stages of sintering. I. Computation of equilibrium surfaces. *Acta Metall. Mater.*, 1994, **42**, 435.
37. Kanters, H., Eisele, U. and Rodel, J., Cosintering simulation and experimentation: case study of nanocrystalline zirconia. *J. Am. Ceram. Soc.*, 2001, **84**, 2757.
38. Bordia, R. K., Zuo, R., Guillon, O., Salamone, S. M. and Rodel, J., Anisotropic constitutive laws for sintering bodies. *Acta Mater.*, 2006, **54**, 111.
39. Aahmy, A. A. and Ragai, A. N., Thermal-expansion behavior of two-phase solids. *J. Appl. Phys.*, 1970, **41**, 5108.
40. Liu, D.-M. and Winn, E. J., Microstresses in particulate-reinforced brittle composites. *J. Mater. Sci.*, 2001, **36**, 3487.
41. Spriggs, R. M., Expression for effect of porosity on elastic modulus of polycrystalline refractory materials, particularly aluminum oxide. *J. Am. Ceram. Soc.*, 1961, **44**, 628.
42. Knudsen, F. P., Dependence of mechanical strength in brittle polycrystalline specimens on porosity and grain size. *J. Am. Ceram. Soc.*, 1959, **42**, 376.
43. Mccolm, I. J., *Ceramic Hardness*. Plenum Press, New York, 1990, p. 276.
44. Kingery, W. D., *Introduction to Ceramics*. John Wiley & Sons Inc., 1975, p. 595.
45. Mccolm, I. J., *Ceramic Hardness*. Plenum Press, New York, 1990, p. 8.